



Stable isotopic results from paleosol carbonate in South Asia: Paleoenvironmental reconstructions and selective alteration

Andrew Leier*, Jay Quade, P. DeCelles, P. Kapp

Department of Geosciences, University of Arizona, Tucson, AZ 85721, United States

ARTICLE INFO

Article history:

Received 2 June 2008

Received in revised form 17 November 2008

Accepted 30 December 2008

Available online 13 February 2009

Editor: P. DeMenocal

Keywords:

oxygen isotope
carbon isotope
paleosol carbonate
marine carbonate
paleoelevation

ABSTRACT

We measured $\delta^{18}\text{O}$ and $\delta^{13}\text{C}$ values of paleosol carbonate nodules from a variety of sedimentary units in southern Asia in order to reconstruct paleoenvironmental conditions and to evaluate for possible diagenetic alteration. Paleosol carbonate nodules were collected from Lower to Upper Cretaceous strata exposed in two locations in southern Tibet, and from Lower to Middle Miocene strata in northern India and Nepal. Additional samples were collected from stratigraphically adjacent marine carbonate units to test for possible resetting of stable isotope values. Based on the implausibly low $\delta^{18}\text{O}$ values ($\sim -13\%$) of most of the marine carbonate samples, we interpret the $\delta^{18}\text{O}$ values of the associated paleosol carbonate nodules as being reset, and therefore unreliable for paleoenvironmental or paleoelevation reconstruction. Importantly, the $\delta^{18}\text{O}$ values of both marine and nonmarine carbonate samples have been altered irrespective of texture, including micritic fabrics, suggesting textural criteria alone are insufficient to determine whether primary stable isotope values have been altered. In contrast, $\delta^{13}\text{C}$ values of marine carbonate rocks fall within the expected primary isotopic range, and so by association we interpret the $\delta^{13}\text{C}$ values of paleosol carbonate from the same sections to have been unaffected by diagenesis. Using the $\delta^{13}\text{C}$ values of paleosol carbonate nodules from Cretaceous strata in southern Tibet, atmospheric $p\text{CO}_2$ is estimated to have been 1400–2000 ppmV between 130–120 Ma, and 2600–3200 ppmV between 100–90 Ma, consistent with previous estimates of $p\text{CO}_2$ for these time periods. Paleosol carbonate nodules within early to middle Miocene strata in northern India and Nepal have average $\delta^{13}\text{C}$ values of -10.4% , indicating virtually pure C_3 vegetation and lower $p\text{CO}_2$.

© 2009 Elsevier B.V. All rights reserved.

1. Introduction

Carbon and oxygen isotopes of paleosol carbonate nodules are powerful tools in the reconstruction of several aspects of past environments, including temperature (Ghosh et al., 2006), $p\text{CO}_2$ (Cerling, 1992; Ekart et al., 1999), vegetation (Cerling et al., 1989), and elevation (Garzione et al., 2000). In the latter case, such reconstructions are critical for understanding how mountain belts and plateaus form, and therefore are increasingly important in many tectonic investigations. The different processes thought to produce high elevations, such as upper crustal thickening and lithospheric mantle delamination, should yield differing paleoelevation histories (Molnar et al., 1993; Tapponnier et al., 2001). Thus, by providing a record of the timing and magnitude of surface uplift, oxygen isotope paleoaltimetry provides one of the few means by which large-scale tectonic and geodynamic hypotheses can be evaluated.

A crucial precondition of carbonate-based oxygen isotope paleoaltimetry and other paleoenvironmental reconstructions is that the $\delta^{18}\text{O}$

and $\delta^{13}\text{C}$ values (versus VPDB, in ‰) of the carbonate are primary and have not been altered. This assumption has yet to be rigorously tested for most paleosol carbonate nodules, but in the case of marine carbonate, ample evidence suggests diagenetic resetting of primary isotopic compositions—especially oxygen—is widespread. Primary $\delta^{18}\text{O}$ values of marine carbonate are limited to a narrow range, generally between 0 and -4% (Veizer et al., 1999). The fact that ancient marine carbonates commonly have $\delta^{18}\text{O}$ values that fall well outside of this range indicate $\delta^{18}\text{O}$ values are often reset during burial and diagenesis (Dickson and Coleman, 1980). By contrast, $\delta^{13}\text{C}$ values of marine carbonates are much more resistant to alteration, permitting reconstruction of the $\delta^{13}\text{C}$ values of marine dissolved inorganic carbon well back into the Proterozoic (Kaufman and Knoll, 1995).

Determining if $\delta^{18}\text{O}$ and $\delta^{13}\text{C}$ values of paleosol carbonate nodules have been reset during diagenesis is more difficult than with marine carbonate. Unlike marine carbonate, the wide range of commonly observed primary $\delta^{18}\text{O}$ (~ -20 to $+10\%$) and $\delta^{13}\text{C}$ values (~ -14 to $+4\%$) of soil carbonate make detection of diagenetic effects difficult. Textural characteristics often serve as a first-order criteria for selecting unaltered paleosol carbonate. The preservation of micrite and the absence of obvious recrystallization should indicate relatively little diagenetic alteration has occurred and that the measured $\delta^{18}\text{O}$ and $\delta^{13}\text{C}$ values are primary. The question of whether paleosol carbonate

* Corresponding author. Current address: Department of Geoscience, University of Calgary, Calgary, AB Canada T2N 1N4.

E-mail address: aleier@ucalgary.ca (A. Leier).



Fig. 1. Location of sampled stratigraphy and areas referred to in the text. Grey shading indicates the Himalaya Range. Cretaceous carbonate strata were sampled from southern Tibet at Duba and Penbo. Miocene carbonates were sampled from Subathu in India and Swat Khola and Pathu Khola in Nepal. Carbonates sampled in Nima and the Siwalik Group in Pakistan are discussed in the Implications and Recommendations Section.

$\delta^{18}\text{O}$ values are altered is by no means trivial in that these data are often critical to evaluating entire tectonic and geodynamic models of plateau and orogenic growth (e.g., Rowley and Currie, 2006).

We measured $\delta^{18}\text{O}$ and $\delta^{13}\text{C}$ values of paleosol carbonate nodules from several stratigraphic successions in southern Asia in order to reconstruct paleoenvironmental conditions and to investigate the fidelity of the stable isotope record of paleosol carbonate nodules (Fig. 1). The locations were specifically chosen because they contain marine carbonate units interstratified with nonmarine successions

containing paleosol carbonate nodules. Unaltered marine carbonate have $\delta^{18}\text{O}$ and $\delta^{13}\text{C}$ values that fall within a limited range (e.g., Veizer et al., 1999), thus the marine carbonate provide control points that can be used to determine if the $\delta^{18}\text{O}$ and $\delta^{13}\text{C}$ values of the adjacent paleosol carbonate nodules are primary or altered. This methodology avoids potential problems that may arise by using textural or cathodoluminescence techniques to test for diagenesis (e.g., Rush and Chafetz, 1990). Samples were analyzed and thin-sectioned from Cretaceous strata in southern Tibet and early-middle Miocene strata

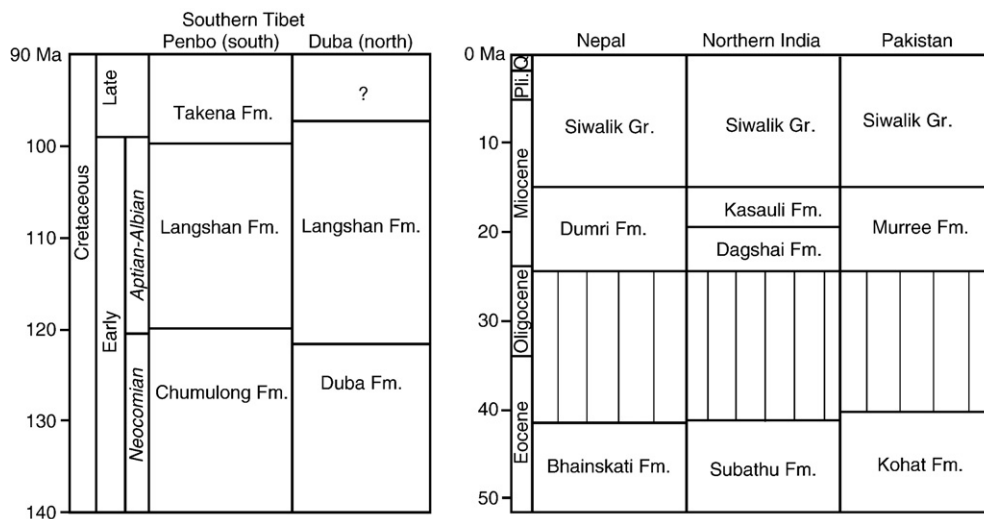


Fig. 2. Regional stratigraphic framework of the sampled rocks. (a) Sampled rock units in southern Tibet consist of the nonmarine Duba Formation (north), the marine Langshan Formation (north and south), and the nonmarine Takena Formation (south). (b) Sampled rock units in the Himalayan foreland consist of the marine Subathu Formation and the nonmarine Dagshai Formation (both in India), and the nonmarine Dumri Formation (Nepal).

Table 1
Tibet samples

Sample	$\delta^{13}\text{C}$ (VPDB)	$\delta^{18}\text{O}$ (VPDB)	Facies	Sample type	Formation	Section-height (m)	Latitude (N)	Longitude (E)
<i>Penbo study area (south)</i>								
PB-3-8A	1.28	-13.68	Marine	Matrix-micrite	Takena	PB3-8m	29 58.117	91 16.486
PB-3-8B	1.26	-13.18	Marine	Shell material	Takena	PB3-8m	29 58.117	91 16.486
PB-3-8C	1.33	-13.40	Marine	Matrix-micrite	Takena	PB3-8m	29 58.117	91 16.486
PB-3-8D	1.21	-13.32	Marine	Shell material	Takena	PB3-8m	29 58.117	91 16.486
PB3-8	1.19	-14.23	Marine	Matrix-micrite	Takena	PB3-8m	29 58.117	91 16.486
PB3-8	0.86	-15.18	Marine	Sparite vein	Takena	PB3-8m	29 58.117	91 16.486
PB3-8	1.51	-13.38	Marine	Shell material	Takena	PB3-8m	29 58.117	91 16.486
PB3-8	2.08	-13.01	Marine	Shell material	Takena	PB3-8m	29 58.117	91 16.486
PB-5-32A	0.09	-13.18	Marine	Matrix-micrite	Takena	PB5-32m	29 55.447	91 16.981
PB-5-32B	-0.01	-13.16	Marine	Matrix-micrite	Takena	PB5-32m	29 55.447	91 16.981
PB-5-32C	0.82	-13.50	Marine	Shell material	Takena	PB5-32m	29 55.447	91 16.981
PB-5-32D	0.48	-13.16	Marine	Shell material	Takena	PB5-32m	29 55.447	91 16.981
PB5-32	-1.62	-12.72	Estuarine	Shell material	Takena	PB5-32m	29 55.447	91 16.981
PB5-32	0.32	-12.82	Estuarine	Matrix-micrite	Takena	PB5-32m	29 55.447	91 16.981
PB5-32	-0.31	-10.48	Estuarine	Sparite vein	Takena	PB5-32m	29 55.447	91 16.981
JPB-1A	2.58	-13.12	Marine	Shell material	Takena	Penbo section	29 55.700	91 21.228
JPB-1B	0.64	-13.99	Marine	Matrix-micrite	Takena	Penbo section	29 55.700	91 21.228
JPB-2A	1.46	-13.10	Marine	Shell material	Takena	Penbo section	29 55.713	91 21.168
JPB-2B	0.14	-13.50	Marine	Matrix-micrite	Takena	Penbo section	29 55.713	91 21.168
JPB-2C	1.26	-13.04	Marine	Shell material	Takena	Penbo section	29 55.713	91 21.168
JPB-16A	-2.47	-12.03	Marine	Shell material	Takena	Penbo section	29 58.321	91 16.454
JPB-16B	0.50	-12.81	Marine	Matrix-micrite	Takena	Penbo section	29 58.321	91 16.454
PB-3-186A	-6.75	-13.96	Paleosol	Matrix-micrite	Takena	PB3-186m	29 58.287	91 16.519
PB-3-186B	-6.25	-13.32	Paleosol	Matrix-micrite	Takena	PB3-186m	29 58.287	91 16.519
PB-3-186C	-7.05	-13.66	Paleosol	Matrix-micrite	Takena	PB3-186m	29 58.287	91 16.519
PB-3-186D	-6.79	-13.97	Paleosol	Matrix-micrite	Takena	PB3-186m	29 58.287	91 16.519
PB3-186	-6.66	-12.94	Paleosol	Matrix-micrite	Takena	PB3-186m	29 58.287	91 16.519
PB3-186	-6.84	-13.16	Paleosol	Matrix-micrite	Takena	PB3-186m	29 58.287	91 16.519
PB3-186	-6.53	-12.97	Paleosol	Matrix-micrite	Takena	PB3-186m	29 58.287	91 16.519
PB3-186	-6.56	-12.88	Paleosol	Matrix-micrite	Takena	PB3-186m	29 58.287	91 16.519
PB3-186	-6.06	-16.93	Paleosol	Sparite vein	Takena	PB3-186m	29 58.287	91 16.519
PB3-186	-5.80	-15.15	Paleosol	Sparite vein	Takena	PB3-186m	29 58.287	91 16.519
JPB-4B	-7.07	-13.85	Paleosol	Matrix-micrite	Takena	Penbo section	29 55.554	91 22.521
JPB-5A	-2.49	-16.90	Paleosol	Matrix-micrite	Takena	Penbo section	29 55.554	91 22.521
JPB-5B	-2.63	-16.29	Paleosol	Matrix-micrite	Takena	Penbo section	29 55.554	91 22.521
JPB-6A	-7.42	-13.91	Paleosol	Matrix-micrite	Takena	Penbo section	29 55.554	91 22.521
JPB-6B	-6.24	-14.08	Paleosol	Matrix-micrite	Takena	Penbo section	29 55.554	91 22.521
JPB-8A	-5.05	-13.96	Paleosol	Matrix-micrite	Takena	Penbo section	29 55.555	91 20.730
JPB-8B	-5.35	-14.00	Paleosol	Matrix-micrite	Takena	Penbo section	29 55.555	91 20.730
JPB-10A	-8.75	-13.89	Paleosol	Matrix-micrite	Takena	Penbo section	29 58.321	91 16.454
JPB-10B	-4.90	-14.00	Paleosol	Matrix-micrite	Takena	Penbo section	29 58.321	91 16.454
JPB-11A	-7.08	-13.75	Paleosol	Matrix-micrite	Takena	Penbo section	29 58.321	91 16.454
JPB-11B	-7.02	-13.38	Paleosol	Matrix-micrite	Takena	Penbo section	29 58.321	91 16.454
JPB-12A	-6.64	-12.99	Paleosol	Matrix-micrite	Takena	Penbo section	29 58.321	91 16.454
JPB-12B	-6.92	-13.44	Paleosol	Matrix-micrite	Takena	Penbo section	29 58.321	91 16.454
JPB-13A	-6.58	-13.34	Paleosol	Matrix-micrite	Takena	Penbo section	29 58.321	91 16.454
JPB-13B	-6.88	-13.08	Paleosol	Matrix-micrite	Takena	Penbo section	29 58.321	91 16.454
JPB-13C	-3.58	-15.15	Paleosol	Matrix-micrite	Takena	Penbo section	29 58.321	91 16.454
JPB-13D	-6.84	-13.31	Paleosol	Matrix-micrite	Takena	Penbo section	29 58.321	91 16.454
PB1-0	-3.45	-12.63	Lacustrine	Matrix-micrite	Takena	PB1-0m	29 55.200	91 15.180
PB1-0	-3.07	-13.01	Lacustrine	Matrix-micrite	Takena	PB1-0m	29 55.200	91 15.180
PB6-84	-5.61	-12.75	Lacustrine	Matrix-micrite	Takena	PB6-84m	29 56.899	91 12.707
PB6-84	-5.95	-12.85	Lacustrine	Matrix-micrite	Takena	PB6-84m	29 56.899	91 12.707
JPB-9A	-8.13	-14.01	Fluvial	Nodule in ss	Takena	Penbo section	29 55.532	91 20.859
JPB-9B	-9.01	-13.56	Fluvial	Nodule in ss	Takena	Penbo section	29 55.532	91 20.859
JPB-15A	-6.89	-13.40	Fluvial	Nodule in ss	Takena	Penbo section	29 58.321	91 16.454
JPB-15B	-6.85	-13.36	Fluvial	Nodule in ss	Takena	Penbo section	29 58.321	91 16.454
JPB-3A	-1.18	-22.78	Fault	Slickenside	n/a	Penbo section	29 55.713	91 21.168
JPB-3B	-1.40	-21.93	Fault	Slickenside	n/a	Penbo section	29 55.713	91 21.168
AB5A	3.23	-7.54	Marine	Matrix-micrite	Jurassic	n/a	30 02.259	91 16.393
AB5B	3.37	-7.91	Marine	Matrix-micrite	Jurassic	n/a	30 02.259	91 16.393
AB5C	3.27	-8.58	Marine	Matrix-micrite	Jurassic	n/a	30 02.259	91 16.393
AB5D	3.14	-8.39	Marine	Matrix-micrite	Jurassic	n/a	30 02.259	91 16.393
MQ-1-11A	1.12	-15.21	Estuarine	Matrix-micrite	Takena	MQ1-11m	29 49.751	90 45.728
MQ-1-11B	0.88	-15.36	Estuarine	Matrix-micrite	Takena	MQ1-11m	29 49.751	90 45.728
MQ-1-11C	0.98	-15.39	Estuarine	Matrix-micrite	Takena	MQ1-11m	29 49.751	90 45.728
MQ-1-11D	1.53	-14.37	Estuarine	Shell material	Takena	MQ1-11m	29 49.751	90 45.728
MQ1-11	0.42	-14.39	Estuarine	Shell material	Takena	MQ1-11m	29 49.751	90 45.728
MQ1-11	1.09	-13.57	Estuarine	Shell material	Takena	MQ1-11m	29 49.751	90 45.728
MQ1-11	0.94	-14.30	Estuarine	Matrix-micrite	Takena	MQ1-11m	29 49.751	90 45.728
MQ1-11	0.33	-16.90	Estuarine	Sparite vein	Takena	MQ1-11m	29 49.751	90 45.728
MQ-3X-2A	-3.90	-14.72	Marine	Matrix-micrite	Takena	MQ3x-2m	29 58.326	90 45.739
MQ-3X-2B	-4.09	-14.85	Marine	Matrix-micrite	Takena	MQ3x-2m	29 58.326	90 45.739

Table 1 (continued)

Sample	$\delta^{13}\text{C}$ (VPDB)	$\delta^{18}\text{O}$ (VPDB)	Facies	Sample type	Formation	Section-height (m)	Latitude (N)	Longitude (E)
<i>Penbo study area (south)</i>								
MQ-3X-2C	-3.97	-14.87	Marine	Matrix-micrite	Takena	MQ3x-2m	29 58.326	90 45.739
MQ-3X-2D	-4.12	-20.92	Marine	Sparite vein	Takena	MQ3x-2m	29 58.326	90 45.739
MQ3X-2	-3.38	-14.43	Marine	Shell material	Takena	MQ3x-2m	29 58.326	90 45.739
MQ3X-2	-4.03	-14.58	Marine	Matrix-micrite	Takena	MQ3x-2m	29 58.326	90 45.739
MQ3X-2	-3.80	-14.62	Marine	Shell material	Takena	MQ3x-2m	29 58.326	90 45.739
MQ3X-2	-6.26	-21.76	Marine	Sparite vein	Takena	MQ3x-2m	29 58.326	90 45.739
MQ3X-2	-4.64	-19.63	Marine	Sparite vein	Takena	MQ3x-2m	29 58.326	90 45.739
MQ3X-2	-4.37	-14.64	Marine	Shell material	Takena	MQ3x-2m	29 58.326	90 45.739
MQ-5-62A	-2.97	-18.09	Paleosol	Matrix-micrite	Takena	MQ5-62m	29 55.885	90 43.601
MQ-5-62B	-3.11	-18.15	Paleosol	Matrix-micrite	Takena	MQ5-62m	29 55.885	90 43.601
MQ-5-62C	-3.22	-18.20	Paleosol	Matrix-micrite	Takena	MQ5-62m	29 55.885	90 43.601
MQ-5-62D	-3.16	-18.05	Paleosol	Matrix-micrite	Takena	MQ5-62m	29 55.885	90 43.601
MQ5-62	-6.85	-11.39	Paleosol	Matrix-micrite	Takena	MQ5-62m	29 55.885	90 43.601
NM2-410A	0.32	-12.85	Marine	Matrix-micrite	Takena	NM2-410m	30 35.795	90 48.490
NM2-410B	0.40	-13.33	Marine	Matrix-micrite	Takena	NM2-410m	30 35.795	90 48.490
NM2-410C	0.43	-13.26	Marine	Matrix-micrite	Takena	NM2-410m	30 35.795	90 48.490
AB-10	-1.73	-18.46	Marine	Sparite vein	Langshan	n/a	30 42.511	91 05.389
AB-10	1.27	-19.61	Marine	Sparite vein	Langshan	n/a	30 42.511	91 05.389
AB-10	0.97	-15.45	Marine	Matrix-micrite	Langshan	n/a	30 42.511	91 05.389
<i>Duba study area (north)</i>								
DB-5-246A	4.79	-5.40	Marine	Matrix-micrite	Langshan	DB5-246m	31 26.385	89 35.165
DB-5-246B	4.87	-4.86	Marine	Matrix-micrite	Langshan	DB5-246m	31 26.385	89 35.165
DB-5-246C	4.75	-5.52	Marine	Shell material	Langshan	DB5-246m	31 26.385	89 35.165
DB-5-246D	4.72	-17.31	Marine	Sparite vein	Langshan	DB5-246m	31 26.385	89 35.165
DB5-246	4.49	-5.74	Marine	Shell material	Langshan	DB5-246m	31 26.385	89 35.165
DB5-246	4.85	-4.41	Marine	Matrix-micrite	Langshan	DB5-246m	31 26.385	89 35.165
DB5-246	4.80	-4.82	Marine	Shell material	Langshan	DB5-246m	31 26.385	89 35.165
DB5-246	4.69	-5.60	Marine	Shell material	Langshan	DB5-246m	31 26.385	89 35.165
DB5-246A	4.65	-5.07	Marine	Matrix-micrite	Langshan	DB5-246m	31 26.385	89 35.165
DB5-246B	4.76	-4.95	Marine	Matrix-micrite	Langshan	DB5-246m	31 26.385	89 35.165
DB5-75A	2.51	-10.76	Marine	Shell material	Langshan	DB5-75m	31 26.477	89 35.208
DB5-75B	4.27	-7.01	Marine	Shell material	Langshan	DB5-75m	31 26.477	89 35.208
DB5-75C	3.07	-19.21	Marine	Sparite vein	Langshan	DB5-75m	31 26.477	89 35.208
DB5-75D	4.14	-8.16	Marine	Matrix-micrite	Langshan	DB5-75m	31 26.477	89 35.208
DB1-27A	-13.11	-13.36	Paleosol	Matrix-micrite	Duba	DB1-27m	31 24.609	89 42.562
DB1-27B	-13.16	-13.60	Paleosol	Matrix-micrite	Duba	DB1-27m	31 24.609	89 42.562
DB1-27C	-12.61	-14.03	Paleosol	Matrix-micrite	Duba	DB1-27m	31 24.609	89 42.562
DB-4-11A	-7.36	-11.21	Paleosol	Matrix-micrite	Duba	DB4-11m	31 26.822	89 35.095
DB-4-11B	-7.41	-11.55	Paleosol	Matrix-micrite	Duba	DB4-11m	31 26.822	89 35.095
DB-4-11C	-8.48	-10.62	Paleosol	Matrix-micrite	Duba	DB4-11m	31 26.822	89 35.095
DB-4-11D	-7.55	-12.47	Paleosol	Matrix-micrite	Duba	DB4-11m	31 26.822	89 35.095
DB4-11	-6.85	-7.26	Paleosol	Spar cement	Duba	DB4-11m	31 26.822	89 35.095
DB4-11	-6.89	-12.45	Paleosol	Matrix-micrite	Duba	DB4-11m	31 26.822	89 35.095
DB4-11	-6.89	-11.73	Paleosol	Matrix-micrite	Duba	DB4-11m	31 26.822	89 35.095
DB4-11	-7.04	-12.29	Paleosol	Matrix-micrite	Duba	DB4-11m	31 26.822	89 35.095
DB4-11	-7.05	-12.22	Paleosol	Matrix-micrite	Duba	DB4-11m	31 26.822	89 35.095
DB4-11A	-7.29	-12.12	Paleosol	Matrix-micrite	Duba	DB4-11m	31 26.822	89 35.095
DB4-11B	-7.26	-11.95	Paleosol	Matrix-micrite	Duba	DB4-11m	31 26.822	89 35.095
DB-6-11A	-7.30	-7.14	Paleosol	Matrix-micrite	Duba	DB6-11m	31 24.554	89 42.825
DB-6-11B	-7.22	-7.12	Paleosol	Matrix-micrite	Duba	DB6-11m	31 24.554	89 42.825
DB-6-11C	-7.25	-6.90	Paleosol	Matrix-micrite	Duba	DB6-11m	31 24.554	89 42.825
DB-6-11D	-7.29	-7.74	Paleosol	Matrix-micrite	Duba	DB6-11m	31 24.554	89 42.825
DB6-11	-7.37	-5.00	Paleosol	Matrix-micrite	Duba	DB6-11m	31 24.554	89 42.825
DB6-11A	-7.04	-6.75	Paleosol	Matrix-micrite	Duba	DB6-11m	31 24.554	89 42.825
DB6-11B	-7.08	-6.71	Paleosol	Matrix-micrite	Duba	DB6-11m	31 24.554	89 42.825
LP-3-20A	3.19	-11.73	Marine	Matrix-micrite	Langshan	LP3-20m	31 52.548	89 34.202
LP-3-20B	3.10	-11.46	Marine	Matrix-micrite	Langshan	LP3-20m	31 52.548	89 34.202
LP-3-20C	2.98	-10.11	Marine	Matrix-micrite	Langshan	LP3-20m	31 52.548	89 34.202
LP-3-20D	3.52	-4.34	Marine	Shell material	Langshan	LP3-20m	31 52.548	89 34.202
LP3-20	1.95	-13.09	Marine	Weathering rind	Langshan	LP3-20m	31 52.548	89 34.202
LP3-20	3.44	-4.44	Marine	Spar cement	Langshan	LP3-20m	31 52.548	89 34.202
LP3-20	2.74	-10.45	Marine	Grain	Langshan	LP3-20m	31 52.548	89 34.202
LP3-20	3.08	-8.38	Marine	Shell material	Langshan	LP3-20m	31 52.548	89 34.202
LP3-20	3.08	-9.45	Marine	Grain	Langshan	LP3-20m	31 52.548	89 34.202
LP3-20	3.11	-10.19	Marine	Grain	Langshan	LP3-20m	31 52.548	89 34.202
LP3-20A	3.18	-11.98	Marine	Matrix-micrite	Langshan	LP3-20m	31 52.548	89 34.202
LP3-20B	3.06	-12.85	Marine	Sparite vein	Langshan	LP3-20m	31 52.548	89 34.202
LP1.15	-5.71	-9.69	Marine	Matrix-micrite	Langshan	LP1-15m	31 49.664	89 37.161
LP4-27A	-3.12	-13.00	Marine	Matrix-micrite	Langshan	LP4-27m	31 54.380	89 37.420
LP4-27B	-3.99	-13.31	Marine	Matrix-micrite	Langshan	LP4-27m	31 54.380	89 37.420
LP5-48A	3.50	-11.87	Marine	Matrix-micrite	Langshan	LP5-48m	n/a	n/a
LP5-48B	3.87	-19.33	Marine	Sparite vein	Langshan	LP5-48m	n/a	n/a

Table 2
Foreland samples

Sample	$\delta^{13}\text{C}$ (VPDB)	$\delta^{18}\text{O}$ (VPDB)	Facies	Sample type	Formation	Section-height (m)	Latitude	Longitude
<i>India</i>								
Kamli								
INACR-VEIN A/INDIA/JQ	-10.27	-17.48	Paleosol	Vein	Dagshai	8	N30°49.859	E76°58.082
INACR-VEIN B/INDIA/JQ	-10.26	-17.36	Paleosol	Vein	Dagshai	8	N30°49.860	E76°58.083
INACR-18A	-10.46	-14.86	Paleosol	Nodule	Dagshai	NA	N30°49.853	E76°58.076
INACR-18B	-10.40	-15.27	Paleosol	Nodule	Dagshai	NA	N30°49.854	E76°58.077
INACR-18C	-10.62	-15.54	Paleosol	Nodule	Dagshai	NA	N30°49.855	E76°58.078
INACR-19A	-10.33	-16.47	Paleosol	Nodule	Dagshai	2	N30°49.856	E76°58.079
INACR-19B/INDIA/JQ	-10.35	-16.48	Paleosol	Nodule	Dagshai	2	N30°49.857	E76°58.080
INACR-19 /INDIA/JQ	-10.44	-15.96	Paleosol	Nodule	Dagshai	2	N30°49.858	E76°58.081
Koshileya Nadi								
INACR-24A/INDIA/JQ	-10.19	-13.69	Paleosol	Nodule	Dagshai	13	N30°51.345	E77°00.400
INACR-24B/INDIA/JQ	-10.39	-13.55	Paleosol	Nodule	Dagshai	13	N30°51.345	E77°00.400
INACR-24C/INDIA/JQ	-10.32	-12.51	Paleosol	Nodule	Dagshai	13	N30°51.345	E77°00.400
INACR-26A/INDIA/JQ	-10.51	-13.39	Paleosol	Nodule	Dagshai	20	N30°51.345	E77°00.400
INACR-26B/INDIA/JQ	-10.63	-12.74	Paleosol	Nodule	Dagshai	20	N30°51.345	E77°00.400
INACR-26C/INDIA/JQ	-10.59	-13.31	Paleosol	Nodule	Dagshai	20	N30°51.345	E77°00.400
INACR-28/INDIA/JQ	-10.74	-12.82	Paleosol	Nodule	Dagshai	32	N30°51.345	E77°00.400
INACR-29B/INDIA/JQ	-10.13	-12.32	Paleosol	Nodule	Dagshai	55	N30°51.345	E77°00.400
INACR-29C/INDIA/JQ	-10.07	-12.53	Paleosol	Nodule	Dagshai	55	N30°51.345	E77°00.400
INACR-31A/INDIA/JQ	-10.70	-13.32	Paleosol	Nodule	Dagshai	73	N30°51.345	E77°00.400
INACR-31B/INDIA/JQ	-10.61	-13.97	Paleosol	Nodule	Dagshai	73	N30°51.345	E77°00.400
INACR-31C/INDIA/JQ	-10.61	-14.68	Paleosol	Nodule	Dagshai	73	N30°51.345	E77°00.400
INACR-33A/INDIA/JQ	-9.40	-9.91	Paleosol	Nodule	Dagshai	121	N30°51.345	E77°00.400
INACR-33B/INDIA/JQ	-10.19	-12.84	Paleosol	Nodule	Dagshai	121	N30°51.345	E77°00.400
INACR-33C/INDIA/JQ	-9.78	-10.63	Paleosol	Nodule	Dagshai	121	N30°51.345	E77°00.400
INACR-14AFORAM/INDIA/JQ	-0.40	-11.07	Marine	Foram	Subathu		N30°51.39	E77°00.346
INACR-14BMATRIX/INDIA/JQ	-2.06	-7.10	Marine	Matrix	Subathu		N30°51.39	E77°00.346
INACR-14CMATRIX/INDIA/JQ	-3.37	-9.88	Marine	Matrix	Subathu		N30°51.39	E77°00.346
INACR-16A/QUADE/	-1.53	-7.21	Marine	Foram	Subathu		N30°51.39	E77°00.346
INACR-16B/QUADE/	-1.57	-5.79	Marine	Foram	Subathu		N30°51.39	E77°00.346
INACR-16C/QUADE/	-1.36	-5.66	Marine	Foram	Subathu		N30°51.39	E77°00.346
INACR-16D/QUADE/	-1.21	-6.27	Marine	Foram	Subathu		N30°51.39	E77°00.346
INACR-16E/QUADE/	-1.44	-7.79	Marine	Foram	Subathu		N30°51.39	E77°00.346
INACR-16F/QUADE/	-1.99	-7.31	Marine	Foram	Subathu		N30°51.39	E77°00.346
INACR-16G/QUADE/	-1.20	-7.13	Marine	Foram	Subathu		N30°51.39	E77°00.346
INACR-16H/QUADE/	-1.23	-6.58	Marine	Foram	Subathu		N30°51.39	E77°00.346
INACR-16I/QUADE/	-1.00	-5.30	Marine	Foram	Subathu		N30°51.39	E77°00.346
INACR-16J/QUADE/	-1.02	-5.31	Marine	Foram	Subathu		N30°51.39	E77°00.346
<i>Nepal</i>								
Pathu Khola								
PK 5D	-11.05	-12.33	Paleosol	Nodule	Dumre		N28°12'51.7"	E82°18.34.1"
PK 5E	-10.21	-14.10	Paleosol	Nodule	Dumre		N28°12'51.7"	E82°18.34.1"
PK5C	-10.67	-11.43	Paleosol	Nodule	Dumre		N28°12'51.7"	E82°18.34.1"
Swat Khola								
ST 675	-10.81	-18.40	Paleosol	Nodule	Dumre	675	N28°42'26.8"	E81°33'3.7"
ST 750	-10.65	-18.33	Paleosol	Nodule	Dumre	750	N28°42'26.8"	E81°33'3.7"
ST 806	-10.29	-17.90	Paleosol	Nodule	Dumre	806	N28°42'26.8"	E81°33'3.7"
ST 930	-10.11	-18.85	Paleosol	Nodule	Dumre	930	N28°42'26.8"	E81°33'3.7"
ST 930	-10.27	-18.54	Paleosol	Nodule	Dumre	930	N28°42'26.8"	E81°33'3.7"
ST 930	-8.81	-8.94	Paleosol	Nodule	Dumre	930	N28°42'26.8"	E81°33'3.7"

from northern India and Nepal (Figs. 1 and 2); details of the specific sampling localities are included in Tables 1 and 2.

2. Setting & sample stratigraphy

2.1. Southern Tibet

The Tibetan Plateau is composed of several continental terranes that accreted onto southern Asia during the Paleozoic and Mesozoic, prior to the Indo-Asian collision (Yin and Harrison, 2000). The southernmost of these terranes is the Lhasa terrane, which collided with southern Asia during Jurassic-Cretaceous time (Dewey et al., 1988; Yin and Harrison, 2000). Carbonate samples were collected from marine and nonmarine Cretaceous strata in two areas within the Lhasa terrane of southern Tibet: Duba in the north, and Penbo in the south (Figs. 1 and 2; Table 1). Cretaceous stratigraphy in the Lhasa terrane consists of Lower Cretaceous terrestrial and marginal marine clastic strata of Neocomian age, Lower Cretaceous marine limestone of Aptian-Albian age (hereafter denoted as

"Aptian-Albian" to distinguish these strata from the underlying Lower Cretaceous clastic units), and Upper Cretaceous fluvial strata (Fig. 2; Yin et al., 1988; Leeder et al., 1988; Leier et al., 2007a). Paleosol carbonate nodules were sampled in the Duba area from the Lower Cretaceous Duba Formation, a > 1 km thick succession of fluvial sandstone and floodplain mudstone (Leeder et al., 1988; Leier et al., 2007b). The paleosols are red to purple in color and contain distinct zones with carbonate nodules (Fig. 3). The approximate depositional age of these deposits is 125 Ma (Leier et al., 2007b). Samples of marine limestone were collected in the same area from Aptian-Albian limestone units that conformably overly the paleosols of the Duba Formation. The marine limestone (>1 km thick Langshan Formation) contain orbitolinid foraminifera and were deposited in muddy lagoonal environments with interspersed rudist patch reefs (Leeder et al., 1988; Leier et al., 2007b). Burial depths of these units are poorly constrained but were likely less than 5 km (Yin et al., 1988).

The sampled strata in the Penbo study area in southern Lhasa consist of the same foraminifera-bearing Aptian-Albian marine limestone along with an overlying succession of Upper Cretaceous

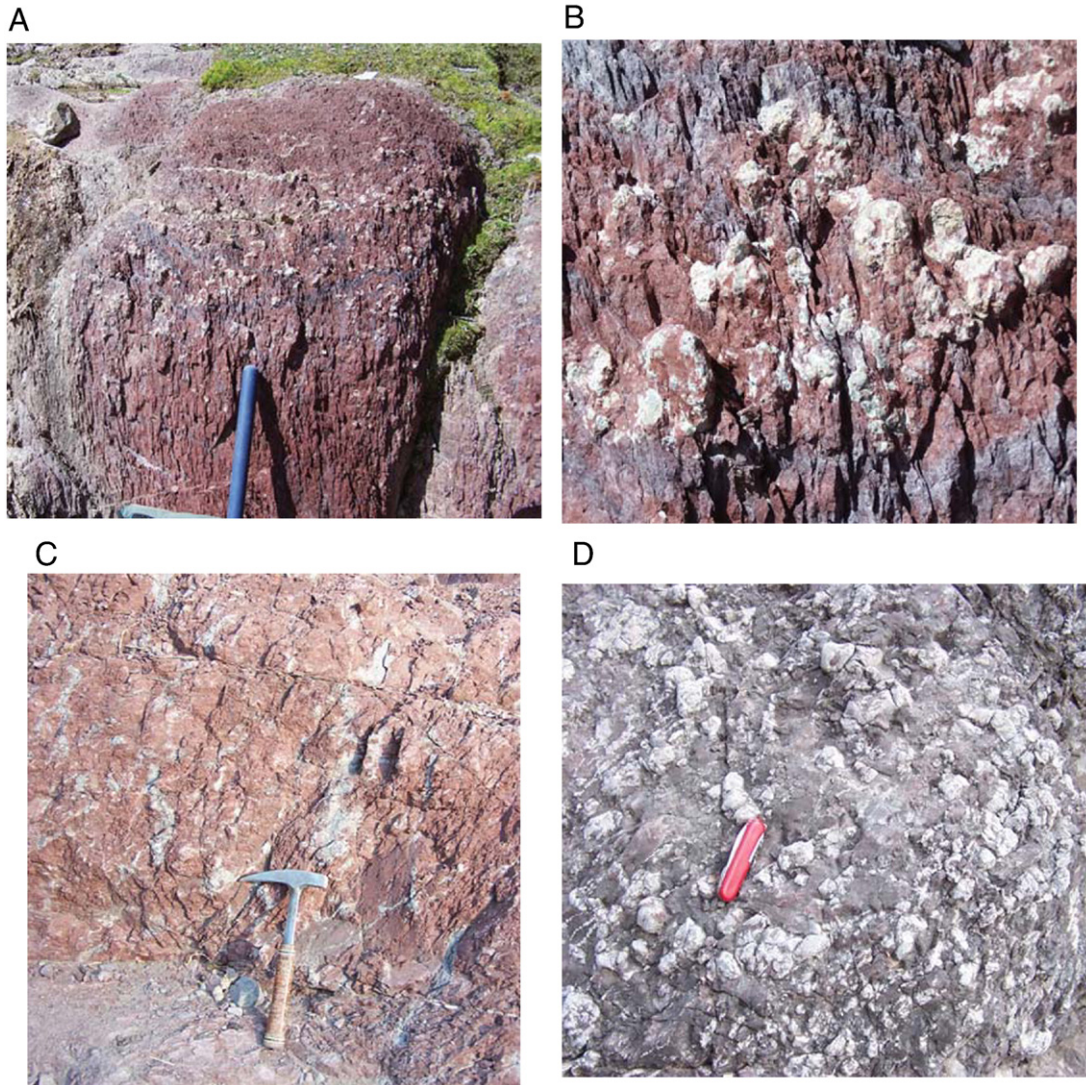


Fig. 3. Photos of the paleosols and sampled carbonate nodules. (A) and (B) Paleosol with carbonate nodules of the Cretaceous Takena Formation in southern Tibet. (C) and (D) Paleosols and carbonate nodules from the Dagshai Formation in India.

nonmarine clastic deposits called the Takena Formation (Yin et al., 1988). The Takena Formation is composed primarily of fluvial sandstone and paleosol units; rare estuarine beds in the lower half of the formation indicate deposition was near sea-level (Leier et al., 2007a). Paleosols in the Penbo study area are red to purple in color, leached free of carbonate in their upper portions and contain dispersed carbonate nodules in their lower halves (Fig. 3). The tops of the paleosols are abrupt; the lower bases grade downwards into parent mudstone. The approximate depositional age of the paleosol carbonate nodules in the Penbo study area is 95 Ma (Leier et al., 2007c). Throughout the succession, carbonate nodules were commonly reworked into contemporaneous channel deposits, which were also sampled. Burial depths of Cretaceous strata are not well constrained but may have been as great as 8–10 km (He et al., 2007; Kapp et al., 2007).

2.2. Foreland samples (India)

The Indo–Asian collision at ca. 55 Ma (e.g., Guillot et al., 2003) and the continued relative northward motion of India formed the Himalaya Range. The crustal load associated with the thickened crust of the Himalaya produced the Himalaya foreland basin, which

has been infilled by sediments derived from the erosion of the adjacent mountains.

We measured and sampled a section that encompasses marine beds of the Early to Middle Eocene Subathu Formation overlain by fluvial deposits of the Dagshai Formation (see Kumar and Loyal, 1987) near the village of Subathu in Himachal Pradesh along Koshileya Nala, in NW India (Fig. 1). We sampled large nummulitic foraminifera (*Asilina spera*) from the upper Subathu Formation and paleosol nodules from the lower Dagshai Formation (Table 2). Like the correlative Dumri Formation in Nepal (see below), the Dagshai Formation represents the earliest stages of molassic deposition into the Himalayan foreland and is thought to be Early to Middle Miocene in age, based on maximum $^{40}\text{Ar}/^{39}\text{Ar}$ ages of 20–22 Ma from detrital muscovite in India (Najman et al., 1997) and Nepal (DeCelles et al., 2001). The paleosols in the Dagshai are abundant and conspicuous for their mottled red color (2.5YR–5YR 4/2d), pervasive bioturbation, leached upper portions, and carbonate nodule-rich lower zones (Fig. 3). Typical paleosols are two to three meters thick. We sampled six paleosols over a ~125 m thickness of Dagshai Formation, and foraminifera approximately 70 m below the base of the Dagshai Formation in the underlying Subathu Formation. We also sampled carbonates from two paleosols in the basal ~20 m of the Dagshai

Formation at the nearby village of Kamli (Table 2). The Dagshai Formation was buried by a minimum of 3 km of late Neogene Siwalik Group sediments (Brozovic and Burbank, 2000) and by a further unknown amount by Lesser Himalayan rocks thrust onto the Dagshai Formation along the Main Boundary Thrust.

2.3. Foreland samples (Nepal)

We sampled paleosol carbonate nodules from the Dumri Formation, which crops out in various isolated locations in the foothills of Nepal (Fig. 1) and is composed of fluvial sandstone interbedded with

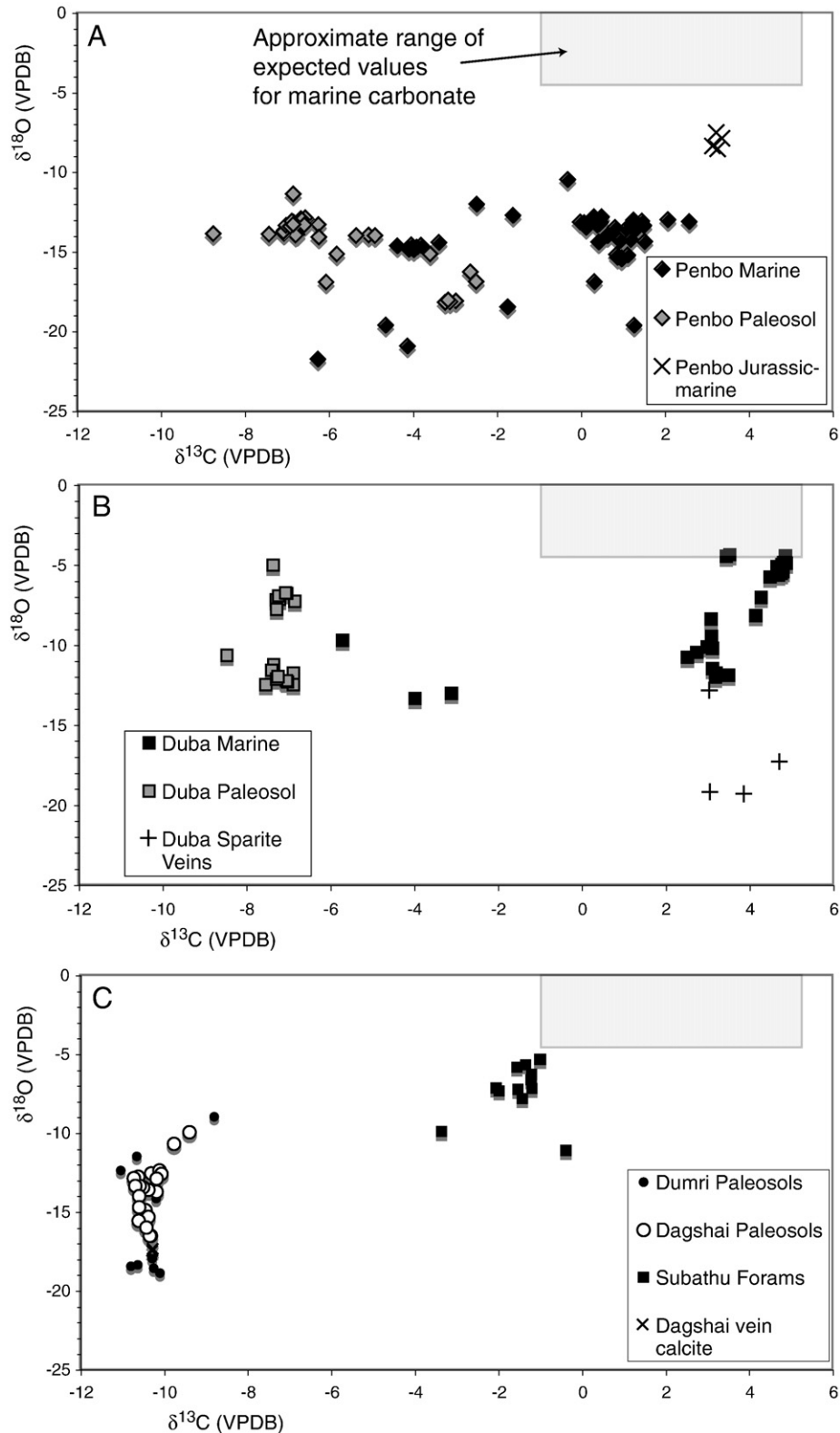


Fig. 4. Results of the stable isotope analyses. (A) Results from the Penbo area in southern Tibet. (B) results from the Duba area in southern Tibet. (C) Results from the samples collected in the foreland strata exposed in India (Subathu and Dagshai Formations) and Nepal (Dumri Formation).

floodplain siltstone. The Dumri Formation rests atop the Middle to Late Eocene-age Bhainskati Formation (Sakai, 1983) and is overlain by the <13 Ma Siwalik Group. Paleomagnetic sampling from Swat Khola (Ojha et al., *in review*) suggests an early Miocene (15–20 Ma) age for the Dumri Formation, consistent with maximum ages of 20–22 Ma from the correlative Dagshai Formation in NW India. The Dumri Formation in western Nepal was deeply buried tectonically by Middle–Late Miocene time. The top of the Dumri Formation at Swat Khola is cut by the Dadeldhura/Ramgahr thrust system. Thrusting commenced 10–14 Ma, emplacing >10 km of Lesser Himalayan crystalline rocks on top of the Dumri Formation, followed by gradual exhumation in Late Miocene and Pliocene time.

We sampled the Dumri Formation in two locations in western Nepal, at Swat Khola northeast of the town of Dadeldhura, and at Pathu Khola in the Tulsipur area (Fig. 1). Paleosols with secondary carbonate nodules are common in the Dumri Formation, as fully described and pictured in DeCelles et al. (DeCelles et al., 1998, their plate 1c, d). We analyzed pedogenic carbonate nodules from throughout the >1 km thick section (see DeCelles et al., 1998, Fig. 6) exposed at Swat Khola. At Pathu Khola, exposure is less continuous and we obtained samples from only two paleosols (Table 1).

3. Methods

For most of the samples, standard petrographic thin sections and matching 300 μm -thick billets were made in order to characterize the carbonate petrography of the samples and to isolate individual microfacies to be analyzed isotopically (see below). The samples from each of the locations contained a variety of carbonate microfacies

including micrite, sparite, sparite veins, recrystallized microsparite (Tables 1 and 2), and in the marine samples, fossilized shell material from several species. These microfacies were mapped in detail prior to being sampled and analyzed.

The oxygen and carbon isotope values of the sampled carbonate were determined for both whole samples and specific portions (“subsamples”) of the individual samples (e.g., Tables 1 and 2). Samples were subsampled using a variety of techniques, including whole-scale fragmentation and spot-drilling. To subsample individual microfacies, the samples were made into 300 μm -thick billets, which were drilled with a 100–300 μm -diameter bit. Prior to analysis, all of the material was heated 3–4 h in a vacuum at 150–200 $^{\circ}\text{C}$. Isotope measurements were made using an automated sample preparation device (Kiel III) that is attached directly to a Finnigan MAT 252 mass spectrometer at the University of Arizona. Measurements of NBS-19 were performed during sample runs to correct for fractionation effects. All carbonate $\delta^{18}\text{O}_c$ and $\delta^{13}\text{C}_c$ values (denoted with subscript “c”) are reported in the familiar δ notation (in ‰) with respect to VPDB, and water $\delta^{18}\text{O}_w$ values (denoted with subscript “w”) with respect to VSMOW.

4. Results

4.1. Tibet samples

The $\delta^{18}\text{O}_c$ values of all marine and nonmarine carbonate from the Duba area of southern Tibet range from –4 to –19‰, but are generally between –5 and –13‰ (Table 1; Fig. 4). Lower Cretaceous paleosol carbonate nodules from Duba have $\delta^{18}\text{O}_c$ values between –5 and

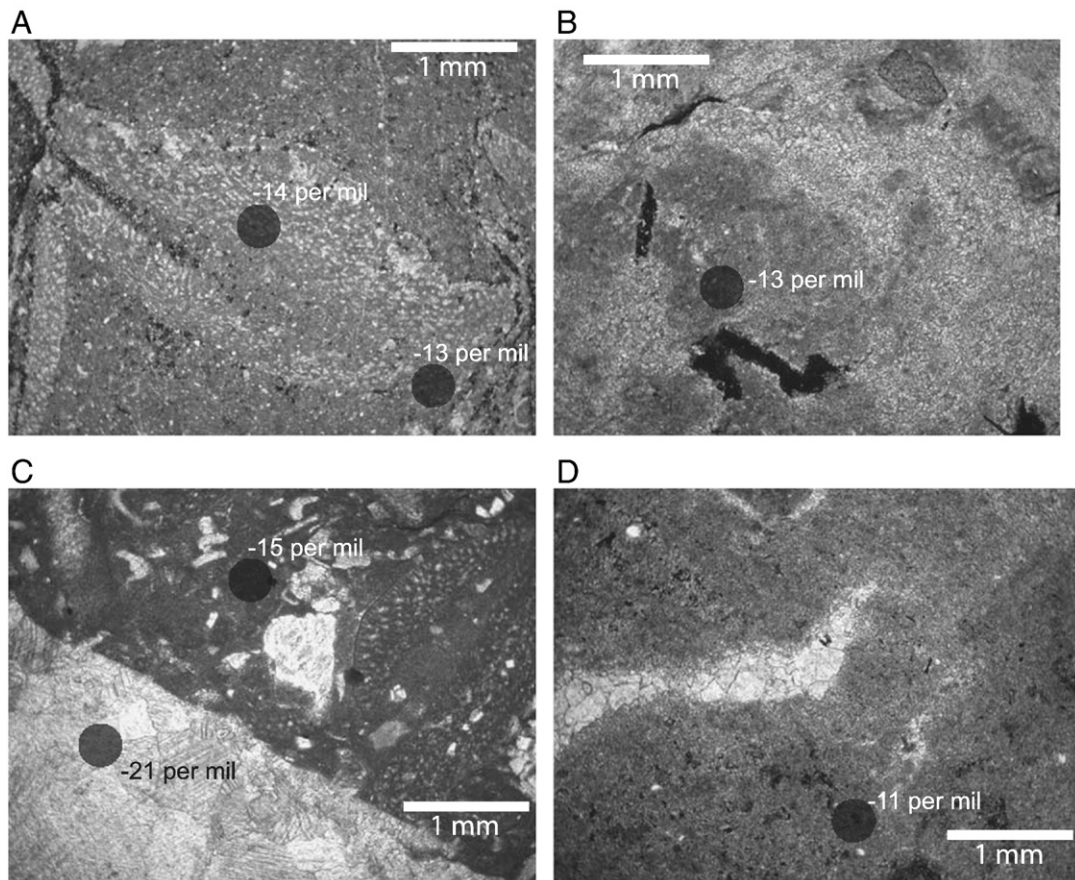


Fig. 5. Images of thin sections of the carbonate sampled in southern Tibet, under cross-polarized light. All images are at the same scale and show the location of a specific fabric that was sampled with a 100–300 μm drill and the $\delta^{18}\text{O}$ value (in ‰, VPDB). (A) shows two sample locations in a Lower Cretaceous orbitolinid limestone. (B) is from a paleosol carbonate nodule with microsparite, micrite and recrystallized micrite. (C) is a sample of marine micrite with bioclasts and a prominent sparite vein. (D) is from a paleosol carbonate nodule with sparite, micrite and recrystallized micrite.

–14‰, whereas Aptian–Albian marine carbonate samples from Duba have $\delta^{18}\text{O}_c$ values typically between –4 and –13‰.

The $\delta^{18}\text{O}_c$ values of all marine and nonmarine carbonate from the Penbo area are generally between –11 to –14‰ and display relatively little variability (Table 1; Fig. 4). Aptian–Albian marine carbonate samples from the Penbo area have $\delta^{18}\text{O}_c$ values between –11 and –14‰. Similarly, Upper Cretaceous paleosol carbonate nodules collected in the Penbo area have $\delta^{18}\text{O}_c$ values of –11 to –14‰. Jurassic marine strata exposed in the Penbo area of southern Lhasa have $\delta^{18}\text{O}_c$ values of ~–8‰, more positive than the Cretaceous marine rocks in the area (Table 1; Fig. 4). The lowest $\delta^{18}\text{O}_c$ value (–22‰) is from calcitic slickensides that are exposed on a fault surface in southern Lhasa.

The $\delta^{13}\text{C}_c$ values of marine rocks sampled in southern Tibet fall (Fig. 4) between 0 and +4‰, whereas nonmarine samples from southern Tibet generally have $\delta^{13}\text{C}_c$ values of –4 to –10‰ (Fig. 4). In the Duba area, Lower Cretaceous paleosol carbonate nodules have $\delta^{13}\text{C}_c$ values of –7 to –13‰, with the majority of values near –7‰ (Table 1). Aptian–Albian marine carbonate samples collected from the Duba area have $\delta^{13}\text{C}_c$ values of +3 to +4‰. In the Penbo study area, Aptian–Albian marine carbonate samples have $\delta^{13}\text{C}_c$ values of 0 to +1‰, and overlying Upper Cretaceous paleosol carbonate samples have values of –6 to –2‰. The $\delta^{13}\text{C}_c$ values of subsamples of sparite veins are typically similar to the $\delta^{13}\text{C}_c$ values of the surrounding non-sparry material. Samples of Jurassic marine strata exposed in the Penbo study area have $\delta^{13}\text{C}_c$ values of ~+3‰.

4.2. Foreland samples

$\delta^{13}\text{C}_c$ values from paleosol carbonates from the Dagshai and Dumri Formations yielded a very uniform $-10.4 \pm 0.3\%$ for India and $-10.5 \pm 0.3\%$ for Nepal (Table 2; Fig. 4). By contrast, $\delta^{18}\text{O}_c$ values of paleosol carbonates proved more variable by section and region. In Nepal, $\delta^{18}\text{O}_c$ values from the Dumri Formation at Pathu Khola were $-12.6 \pm 1.4\%$ compared to $-18.4 \pm 0.3\%$ at Swat Khola. Similarly, $\delta^{18}\text{O}_c$ values from the Dagshai Formation at Kamli in India were -15.9 ± 1.0 , but $-12.8 \pm 1.2\%$ at Koshileya Nala. Sparry calcite-filled tension fractures in one of the Kamli paleosols returned $\delta^{18}\text{O}_c$ values of –17.4 to –17.5‰, slightly lower than the associated soil carbonate nodules. Marine foraminifera from the upper Subathu Formation at Koshileya Nala returned a high $\delta^{18}\text{O}_c$ value of –0.4‰, whereas the enclosing micritic matrix yielded low $\delta^{18}\text{O}_c$ values of –7.1 to –11.1‰. No marine carbonate was available from the Bhainskati Formation in Nepal.

5. Discussion

5.1. Oxygen isotope values

In our view, the $\delta^{18}\text{O}_c$ values of Cretaceous marine carbonate in southern Tibet and Eocene marine carbonate in northern India show strong evidence of resetting. The $\delta^{18}\text{O}_c$ values of the marine carbonate in most sections that we sampled are implausibly low even when considering possible variations in the $\delta^{18}\text{O}_w$ value of ancient seawater (Veizer et al., 1999). For example, at Penbo, marine carbonate, including micritic matrix and shell material, yielded $\delta^{18}\text{O}_c$ values between –12.0 and –16.9‰ (Fig. 5), much lower than expected marine $\delta^{18}\text{O}_c$ values of >–5‰ for the period (Veizer et al., 1999). A few samples of marine units from the Duba area in southern Tibet appear to be the exception to this pattern, and have $\delta^{18}\text{O}_c$ values (~–5‰) that approach those expected in marine carbonate, although most $\delta^{18}\text{O}_c$ values of the marine rocks appear to have been reset (Fig. 4). These findings are consistent with the literature on marine carbonates, where the alteration of primary stable isotope values of has been thoroughly documented (Dickson and Coleman, 1980; Brand and Veizer, 1981; Land, 1986; Choquette and James, 1990; Wenzel, 2000; Rosales et al., 2001; and many others).

By association, we interpret the $\delta^{18}\text{O}_c$ values of the paleosol carbonate nodules collected from stratigraphically adjacent nonmarine deposits to be altered as well, based on the similarity between marine and nonmarine $\delta^{18}\text{O}_c$ values (Fig. 4). Depending on the relative time of resetting, the $\delta^{18}\text{O}_c$ values of the paleosol carbonate nodules may still provide information for paleoelevation and paleoenvironmental reconstructions. We can envision three different alteration scenarios for the paleosol carbonate. The first scenario entails early diagenetic alteration of $\delta^{18}\text{O}_c$ values during early burial and associated with low-temperature interaction with formation waters or different meteoric waters (e.g., Land, 1986) during, for example, short-term sea-level fluctuations or near-surface over-printing (e.g., Deutz et al., 2001). Carbonate in paleosols formed on coastlines, but after permanent shoreline retreat, might not be affected by this process, thus preserving their original $\delta^{18}\text{O}_c$ values. The second scenario involves alteration of $\delta^{18}\text{O}_c$ values during significant burial and at higher temperatures, and the third scenario involves resetting of $\delta^{18}\text{O}_c$ values as strata are exhumed and interact with modern meteoric waters under modern-recent near-surface conditions. Obviously, $\delta^{18}\text{O}_c$ values reset under the second or third scenarios would provide no information on original paleoenvironmental conditions.

Several lines of evidence indicate the $\delta^{18}\text{O}_c$ values of carbonate samples from southern Asia were not reset during the first, “early” scenario. Early alteration of $\delta^{18}\text{O}_c$ values necessarily implies interaction with meteoric or marine waters in coastal environments at relatively low temperatures (<30 °C). Under low-temperature conditions, the $\delta^{18}\text{O}_w$ values of the water needed to reset the $\delta^{18}\text{O}_c$ values of marine carbonate in northern India and southern Tibet would have to have been ~–10 to –20‰ (Kim and O’Neil, 1997). These values are unrealistic given the paleogeographic constraints. In the case of the northern Indian samples, $\delta^{18}\text{O}_w$ values of local meteoric water in New Delhi today is –5.9‰ (VSMOW) (Quade et al., 2007a) and it is likely the $\delta^{18}\text{O}_w$ values of meteoric waters in northern India during Oligo–Miocene time were even higher than today given the lower paleolatitude (Dansgaard, 1964) and presumably higher ambient temperatures. Similarly, Cretaceous meteoric waters with $\delta^{18}\text{O}_w$ values of ~–10 to –20‰ in southern Tibet are unrealistic considering that the area was located at ~10–20°N during the Cretaceous (Besse and Courtillot, 1988) and sedimentary evidence indicates much of the region was near sea-level (Leier et al., 2007a).

The $\delta^{18}\text{O}_c$ values of the samples from southern Asia were most likely reset at relatively higher temperatures during burial or, in the case of the rocks from southern Tibet, possibly during more recent interaction with meteoric waters. The paleo- $\delta^{18}\text{O}_w$ values in Nepal and northern India of >–5.9‰ preclude the possibility that the carbonate in these areas ($\delta^{18}\text{O}_c$ values of ~–12 to –18‰ in northern India and ~–12 to –16‰ in Nepal) have been reset at surface temperatures (Scenario 1 or 3). The $\delta^{18}\text{O}_c$ values of the carbonate must have been altered at higher temperatures (Fig. 6). The strata in Nepal were buried to depths of at least 10 km. Assuming an average geothermal gradient of 25–30 °C/km, these strata could have experienced temperatures of 250 °C.

In Tibet, Scenario 2 (deep alteration) and 3 (recent alteration) are both possible. As in Nepal, strata in the Penbo area of southern Tibet were also buried to depths of ~10 km (Kapp et al., 2007). This would yield sufficiently high (≥ 70 °C) temperatures to produce the observed $\delta^{18}\text{O}_c$ values (~–12‰) from interactions with waters having $\delta^{18}\text{O}_w$ of 0 to –5‰ (Fig. 6).

Alternatively, $\delta^{18}\text{O}_w$ values of meteoric waters in southern Tibet today are very low (Araguas-Araguas et al., 1998; Quade et al., 2007a) leaving open the possibility that $\delta^{18}\text{O}_c$ values in southern Tibet may have been reset relatively recently and at low temperatures (Scenario 3). For example, it is possible to form carbonate with $\delta^{18}\text{O}_c$ values of ~–13‰, like those in the both marine and paleosol carbonates at Penbo, with modern $\delta^{18}\text{O}_w$ values (~–15‰) and mean annual temperatures 8 °C in southern Tibet (IAEA, 2005; Fig. 6).

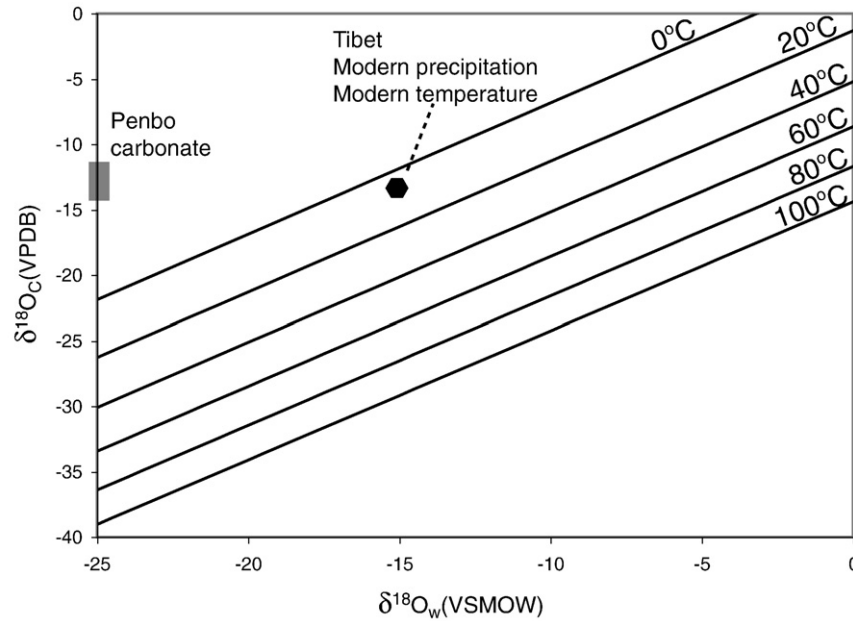


Fig. 6. Graph showing the relationship between $\delta^{18}\text{O}$ values of water, temperature, and the $\delta^{18}\text{O}$ values of carbonate, based on equations of Kim and O'Neil (1997). On the y-axis is highlighted the typical $\delta^{18}\text{O}$ values of carbonate in the Penbo area in southern Tibet. The black node in the graph is placed at the modern mean annual temperature of Lhasa, in southern Tibet, and the $\delta^{18}\text{O}$ value of modern precipitation in the region using Araguas-Araguas et al. (1998) and Quade et al. (2007a). The $\delta^{18}\text{O}$ values of carbonate expected to precipitate under modern conditions in southern Tibet overlap the altered $\delta^{18}\text{O}$ values of the sampled carbonate, suggesting it is possible that the altered $\delta^{18}\text{O}$ values of the Penbo samples were reset relatively recently.

Regardless of which explanation is correct, the $\delta^{18}\text{O}_c$ values of the carbonate in southern Tibet are of no use for surficial paleoenvironmental reconstructions.

5.2. Micrite fabrics and alteration

Developing a fabric-based criteria to independently assess whether oxygen isotope values are original or diagenetically reset would be highly beneficial because carbonate-bearing paleosols are rarely stratigraphically adjacent to marine carbonate. Additionally, techniques commonly used to assess alteration in marine carbonate (e.g., major and minor element geochemistry, cathodoluminescence) are not always foolproof (Rush and Chafetz, 1990; Marshall, 1992) and may not be as applicable to paleosol carbonate nodules. In many instances, evidence of recrystallization can be used as a first-order means of predicting whether $\delta^{18}\text{O}_c$ values have been altered (e.g., Solomon and Walkden, 1985; Wright and Peeters, 1989). Compared to fabrics that clearly indicate later-stage precipitation and recrystallization, like microsparite and sparite veins, finer-grained micritic textures in nonmarine carbonate samples are generally thought to be more reliable recorders of original $\delta^{18}\text{O}_c$ values. However, a growing body of evidence suggests this is not always the case and that even what appears to be original micrite may have altered $\delta^{18}\text{O}_c$ values (e.g., Lee and Hisada, 1999). For example, very low $\delta^{18}\text{O}_c$ values from paleosol carbonate analyzed by Driese et al. (1992) were interpreted as being reset during diagenesis despite the fact that the samples displayed no evidence of recrystallization. Similarly, Garzzone et al. (2004) found that at several sampling sites in southern Tibet, Cenozoic micrite in pedogenic and lacustrine carbonate yielded $\delta^{18}\text{O}_c$ values that were likely altered. Morril and Koch (2002) used differences between $\delta^{18}\text{O}_c$ values of unaltered aragonite and lacustrine micrite to raise the same fidelity issues about the $\delta^{18}\text{O}_c$ values of micrite carbonate.

Our results indicate the presence of micrite in pedogenic carbonate is insufficient, in and of itself, to prove that $\delta^{18}\text{O}_c$ values have not been altered. As discussed above, the low $\delta^{18}\text{O}_c$ values of pedogenic carbonate from Upper Cretaceous strata in the Penbo area of southern

Tibet are interpreted to reflect isotopic resetting. Despite detailed microsampling of these samples, the micrite fabrics yield $\delta^{18}\text{O}_c$ values identical to those of microspar and sparite within the pedogenic carbonate. In the Duba area of southern Tibet, many of the micrite subsamples have low $\delta^{18}\text{O}_c$ values ($\sim -11\%$) strongly suggesting they have been reset. A small number of micrite subsamples from paleosol carbonate nodules in the Duba area have $\delta^{18}\text{O}_c$ values that can be interpreted as original ($\sim -5\%$); however, when viewed within the context of all of the micrite fabrics sampled, these seem to be the exception amongst the micrite samples, and not the rule.

Samples of marine rocks from southern Tibet also indicate little to no correlation between carbonate fabrics and the preservation of original $\delta^{18}\text{O}_c$ values. In the Penbo area, the implausibly low $\delta^{18}\text{O}_c$ values (-13%) of marine micrite clearly indicate these portions of the samples have altered $\delta^{18}\text{O}_c$ values (Fig. 4). Additionally, shell material from foraminifera, bivalves, and echinoids all yield similar $\delta^{18}\text{O}_c$ values of $\sim -13\%$. Several subsamples of micrite in the Duba area have $\delta^{18}\text{O}_c$ values close to those expected for Lower Cretaceous marine rocks, suggesting negligible resetting of $\delta^{18}\text{O}_c$ values (Fig. 4). Once again, however, this appears to be the exception to the general trend.

5.3. Carbon isotopes

There is an extensive literature on marine and nonmarine $\delta^{13}\text{C}_c$ values (Veizer et al., 1999; and many others, Jacobsen and Kaufman, 1999) and the verdict, unlike with $\delta^{18}\text{O}_c$ values, is that diagenetic resetting is much less likely to occur (e.g., Banner and Hanson, 1990; Mora et al., 1996; Tandon and Andrews, 2001). $\delta^{13}\text{C}_c$ values of inorganic carbon in the oceans can be convincingly reconstructed well back into the Proterozoic (e.g., Jacobsen and Kaufman, 1999) provided the carbonates have not experienced decarbonation or exchange at metamorphic temperatures. In the case of our marine samples, samples from both Tibet and India return $\delta^{13}\text{C}_c$ values equal or close to expected marine values. For example, marine carbonate values for 120–100 Ma are -1.9 to $+5.5\%$ at 2σ (Veizer et al., 1999), which overlaps the measured range of $\delta^{13}\text{C}_c$ values of all the marine carbonate grains, fossils, and even most of the micritic cements

from both Penbo and Duba. Similarly, $\delta^{13}\text{C}_c$ values of middle Eocene foraminifera from the Subathu Formation of -0.4% , very close to the expected marine values for this time period of 0 to $+1\%$ (Zachos et al., 2001).

The reasons for contrasting preservation of oxygen versus carbon isotopic compositions are well known and relate to the fact that a typical molar water/rock ratio between natural waters and limestone is 10^3 to 10^4 larger for oxygen than for carbon (Banner and Hanson, 1990). Hence, fluids are far more likely to alter $\delta^{18}\text{O}_c$ than $\delta^{13}\text{C}_c$ values.

5.4. Cretaceous $p\text{CO}_2$

The $\delta^{13}\text{C}_c$ values of ancient paleosol carbonate can be used to estimate ancient $p\text{CO}_2$ values in the atmosphere. The relative contribution of atmospheric CO_2 and soil plant-respired CO_2 can be determined from $\delta^{13}\text{C}_c$ values of soil carbonate using a diffusion-based model originally developed by Cerling (1992). The $\delta^{13}\text{C}_c$ value of soil carbonate is controlled by the $\delta^{13}\text{C}$ value of the soil CO_2 ($\delta^{13}\text{C}_s$), $\delta^{13}\text{C}_s$ in turn varies as a function of the concentration (C_s) and $\delta^{13}\text{C}$ value of soil plant-respired CO_2 ($\delta^{13}\text{C}_{\text{org}}$), and the concentration ($p\text{CO}_2$, denoted as C_a) and $\delta^{13}\text{C}$ value of CO_2 in the atmosphere ($\delta^{13}\text{C}_a$). $S(z)$ is the soil-respired component of soil CO_2 and is defined as $C_s - C_a$, where z is soil depth. Atmospheric $\delta^{13}\text{C}_a$ values are more positive than soil plant-respired $\delta^{13}\text{C}_{\text{org}}$ values; thus, higher $p\text{CO}_2$ values will produce more positive $\delta^{13}\text{C}_s$ values, which in turn will be recorded by soil carbonate as more positive $\delta^{13}\text{C}_c$ values. We reconstructed $p\text{CO}_2$ values using the Cretaceous paleosol carbonate nodules collected in southern Tibet using a linear soil CO_2 production function (Cerling and Quade, 1993; Ekart et al., 1999) and an exponential production function (Quade et al., 2007b) and obtained very similar results. The relationship between C_a and other soil parameters is described by:

$$C_a = S(z) * \frac{^{13}\text{C}_s - 1.0044 * ^{13}\text{C}_{\text{org}} - 4.4}{^{13}\text{C}_a - ^{13}\text{C}_s}$$

where C_a is in ppmV (Ekart et al., 1999). The $\delta^{13}\text{C}_s$ value of ancient soil CO_2 can be reconstructed from measured the $\delta^{13}\text{C}_c$ values of paleosol carbonate nodules, using the temperature-dependent fractionation equation between carbonate and CO_2 of Romanek et al. (1992). Additional information and assumptions used in calculating the $p\text{CO}_2$ values include: carbonate nodules were collected >50 cm below the paleosurface, therefore $S(z) = 5000$ ppmV (Cerling, 1991); ancient $\delta^{13}\text{C}_a$ values are assumed to be near pre-industrial values of $\sim -6.5\%$; $\delta^{13}\text{C}_{\text{org}}$ values = $\delta^{13}\text{C}_a - 18\%$; and paleotemperature is estimated as 25°C based on paleomagnetic data and latitude–temperature correlations (Besse and Courtillot, 1988; Ekart et al., 1999).

Using the average of all of the $\delta^{13}\text{C}_c$ values measured from the paleosol carbonate nodules, atmospheric $p\text{CO}_2$ during the latest Early Cretaceous (paleosols from the Duba study area, 125 Ma) was 1478 ppmV (± 1060 based on 1 standard deviation of $\delta^{13}\text{C}_c$ values), and 3268 (± 1380) ppmV during the earliest Late Cretaceous (paleosols from the Penbo study area, 95 Ma). Using the extreme values, Duba samples (125 Ma) yielded minimum and maximum $p\text{CO}_2$ values of -572 and 2346 ppmV, respectively; Penbo samples (95 Ma) yielded maximum and minimum $p\text{CO}_2$ values of 1103 and 8791 ppmV, respectively. Outlying data points obviously exist within both the Duba and Penbo samples (Table 1). If these values are removed and the average of the remaining values is used to calculate the $p\text{CO}_2$ values, the 125 Ma samples from the Duba area yield an atmospheric $p\text{CO}_2$ value of 2037 (± 278) ppmV, the 95 Ma samples from the Penbo area record $p\text{CO}_2$ values of 2667 (± 786) ppmV.

Key uncertainties not reflected in the errors cited above include paleotemperature uncertainties of 20% that result in $<20\%$ variation in the $p\text{CO}_2$ estimates, and even more critically, the assumed value of $S(z) = 5000$ ppmV. Recent studies of modern soils from New Mexico by Breecker et al. (2007) point to much lower $S(z)$ values, closer to

2000 ppmV during summer when carbonate forms. If representative of Cretaceous soils, then $p\text{CO}_2$ is being seriously overestimated by most studies. Resolution of the most appropriate $S(z)$ value to assume is work in progress. Additional statistical methods can be applied to the data, but given the uncertainties and estimates involved in these calculations we will limit our discussion to these first-order results.

$\delta^{13}\text{C}_s$ values and calculated $p\text{CO}_2$ values of 125 Ma and 95 Ma paleosol nodules from southern Tibet are consistent with previous estimates of Ekart et al. (1999) who obtained $p\text{CO}_2$ values between ~ 1400 and ~ 2700 ppmV, and by Lee and Hisada (1999) from strata of equivalent age in Japan. Similar to Ekart et al. (1999) our calculated $p\text{CO}_2$ values are generally higher than those estimated from other proxies (e.g., Berner and Kothavala, 2001).

The primary difference between our calculated $p\text{CO}_2$ values and previous estimates is in the trend of $p\text{CO}_2$ during middle Cretaceous time. Most reconstructions depict the Cretaceous period as a time during which there was a relatively steady decrease in $p\text{CO}_2$. The paleosol carbonate nodules from southern Tibet have $\delta^{13}\text{C}_c$ values that indicate $p\text{CO}_2$ at ~ 125 Ma was similar to the $p\text{CO}_2$ at ~ 95 Ma. Regardless of the input parameters, it is difficult to reconcile the $\delta^{13}\text{C}_c$ values of the paleosol carbonate nodules with a decrease in $p\text{CO}_2$ between 125 and 95 Ma.

5.5. Early Miocene vegetation

The $\delta^{13}\text{C}_c$ values from the early to mid-Miocene paleosols are a surprisingly uniform -10.4% from Nepal and -10.5% from India. The deeply leached and red appearance of the paleosols suggests relatively high soil respiration rates (>4 mmol/m²/hr). Using the recently revised soil diffusion model (Quade et al., 2007b) this points to a $\delta^{13}\text{C}_c$ value for the paleo-respiratory flux of about -24% at soil temperatures of 30°C , or -25% at 20°C . These values are consistent with a pure or nearly pure cover of C_3 plants. It also suggests that $p\text{CO}_2$ was at or near modern levels (300–800 ppmV, depending on other variables) for this time period, consistent with estimates from other proxies (e.g., Pagani et al., 2005).

The dominance of C_3 biomass for this time period is recognized from some but certainly not all other soil and fossil isotopic records globally. For example, soil carbonate $\delta^{13}\text{C}_c$ records from the mid-western USA (Fox and Koch, 2004) and Africa (Kingston et al., 1994) appear to indicate significant C_4 plant cover (up to 50%). On the other hand, $\delta^{13}\text{C}$ values from fossil teeth point to the dominance of C_3 dietary intake (Cerling et al., 1997), although a small fraction ($<20\%$) of C_4 biomass is permitted by the uncertainties in the $\delta^{13}\text{C}$ value of the dietary end members.

6. Implications and recommendations

Stable isotope data from paleosol carbonate form the basis for many paleoenvironmental reconstructions. The use of $\delta^{18}\text{O}_c$ in reconstructing paleoelevation has received particular focus of late, largely because it provides important constraints for evaluating tectonic and geodynamic models of plateau formation. Indeed, much of the impetus for our investigation came from the possibility of using $\delta^{18}\text{O}_c$ values to reconstruct the paleoelevation history of the Himalayan–Tibetan orogen. Our results, namely the widespread alteration of $\delta^{18}\text{O}_c$ values in paleosol carbonate, highlight an important complication to this approach. Altered $\delta^{18}\text{O}_c$ values of paleosol carbonate are of little use for paleoelevation studies and if not recognized, can lead to erroneous conclusions regarding surface uplift histories (and by extension, tectonic models). In our case, marine carbonate provided a clear means of examining whether $\delta^{18}\text{O}_c$ values had been altered, but in most investigations close association of marine carbonate strata and paleosols is lacking, which raises the question of how to proceed in such situations.

Ideally, paleoelevation investigations using paleosol carbonate $\delta^{18}\text{O}_c$ values should be accompanied by internal tests that can validate the assumption that $\delta^{18}\text{O}_c$ values are unaltered. We have already shown that $\delta^{18}\text{O}_c$ values of any pedogenic texture can be altered and therefore the presence of a particular fabric alone cannot be used as unequivocal proof that samples retain their original $\delta^{18}\text{O}_c$ values.

An alternative approach is suggested by the fact that reworked marine carbonate – ranging from gravel clasts to sandy detritus – is present in many sedimentary sequences, permitting a variation of the sort of test we performed in Tibet and India. We can offer two examples from our own work that demonstrate this approach.

DeCelles et al. (2007) used the $\delta^{18}\text{O}_c$ values of paleosol carbonate nodules in ~25 Ma strata to investigate the paleoelevation history of the Nima Basin in central Tibet (Fig. 1). Based on the low $\delta^{18}\text{O}_c$ values of the paleosol carbonate nodules, DeCelles et al. (2007) concluded that the region had attained its current elevation of ~5 km above sea level by at least 25 Ma. This investigation had to contend with possibility that the $\delta^{18}\text{O}_c$ values were diagenetically altered and had to do so even though there are no marine carbonate strata in the succession that could be used to test for aberrant $\delta^{18}\text{O}_c$ values. Using an “isotopic conglomerate test,” DeCelles et al. (2007) were able to establish the unaltered nature of the paleosol carbonate nodules by sampling the interstratified fluvial sandstone and conglomerate, which contained clasts of marine limestone and soil carbonate nodules. The marine limestone clasts were derived from the weathering and erosion of Cretaceous marine strata in the region, whereas the clasts of soil carbonate were reworked as the paleochannel migrated through the floodplain. The reworked paleosol carbonate nodules have the same $\delta^{18}\text{O}_c$ values as the in-situ paleosol carbonate nodules. Importantly, however, the clasts of marine limestone within the fluvial units have $\delta^{18}\text{O}_c$ (and $\delta^{13}\text{C}$) values consistent with expected values of unaltered marine carbonate stable isotopes and differ markedly from adjacent clasts of reworked paleosol carbonate. If diagenetic resetting of paleosol carbonate $\delta^{18}\text{O}_c$ values had occurred, carbonate of all types should have similar and negative $\delta^{18}\text{O}_c$ values and the marine clasts should not retain their original $\delta^{18}\text{O}_c$ values. The fact that this did not occur provides evidence the very negative $\delta^{18}\text{O}_c$ values of the paleosol carbonate nodules were not due to diagenetic resetting.

The second example comes from Siwalik Group in Pakistan and Nepal (Fig. 1), which represents deposition in the Himalayan foreland by large rivers ancestral to the Indus and Ganges and their large tributaries. Isotopic analysis of the abundant pedogenic carbonate in the Siwaliks has yielded a thirteen million year record of climate and ecologic change (Quade and Cerling, 1995). Unlike the strata in Tibet, the deeper portions of the Siwaliks are no coarser than sand, and hence marine carbonate clasts are not available for testing for isotopic resetting. However, detrital carbonate composes about 3–20% of the detritus in the siltstone and sandstone beds. $\delta^{18}\text{O}_c$ values of this carbonate in uncemented layers ranges from –10 to –13‰, whereas $\delta^{13}\text{C}_c$ values range from –2 to –6‰ (Quade and Roe, 1999). Detrital carbonate of the same average isotopic composition as that found in the Siwalik siltstone is found in modern rivers of the Himalayan foreland. It largely derives from metalimestone and marble in the Tethyan and Lesser Himalaya (Quade et al., 1997). The isotopic compositions of pedogenic and detrital carbonates do not overlap; $\delta^{18}\text{O}_c$ values of pedogenic carbonates are generally higher (–11.5 to –4‰) than in detrital silt (–10 to –13‰) (Quade and Cerling, 1995; Quade et al., 1997).

These are just two examples have how the possibility of diagenesis of paleosol carbonate can be assessed. In using the $\delta^{18}\text{O}_c$ values of deeply buried paleosol carbonates to reconstruct paleoelevation and paleoenvironments, geologists must exercise the same extreme caution as they have shown with interpreting $\delta^{18}\text{O}_c$ values of ancient marine carbonate rocks.

Acknowledgments

We sincerely thank Hema Achythan and Raminder Loyal, and Amanda Reynolds for help with the sections in India, T. P. Ojha for his assistance in Nepal, Din Ling in Tibet, and Shundong He and Dan Eisenberg for their help in Tibet. We appreciate also Dave Dettman's dedication in the lab to producing high-quality analyses in a short time. The manuscript was greatly improved by comments and suggestions from B. Currie and Editor P. deMenocal. We thank R. Scott for help in identifying fossils. Funding for this work came from NSF 0438115 to DeCelles, Kapp, and Quade.

References

- Araguas-Araguas, L., Froehlich, K., Rozanski, K., 1998. Stable isotope composition of precipitation over southeast Asia. *J. Geophys. Res.-Atmos.* 103, 28721–28742.
- Banner, J.L., Hanson, G.N., 1990. Calculation of simultaneous isotopic and trace-element variations during rock–water interaction with applications to carbonate diagenesis. *Geochim. Cosmochim. Acta* 54, 3123–3137.
- Berner, R.A., Kothavala, Z., 2001. GEOCARB III: a revised model of atmospheric CO₂ over phanerozoic time. *Am. J. Sci.* 301, 182–204.
- Besse, J., Courtillot, V., 1988. Paleogeographic maps of the continents bordering the Indian–Ocean since the Early Jurassic. *J. Geophys. Res.-Solid Earth Planets* 93, 11791–11808.
- Brand, U., Veizer, J., 1981. Chemical diagenesis of a multicomponent carbonate system. 2: stable isotopes. *J. Sediment. Petrol.* 51, 987–997.
- Breecker, D., Sharp, Z., McFadden, L., 2007. Extreme conditions of pedogenic carbonate formation and implications for paleoenvironmental reconstruction and paleosol pCO₂ barometry. *Abstr. programs - Geol. Soc. Am.* 39, 182.
- Brozovic, N., Burbank, D.W., 2000. Dynamic fluvial systems and gravel progradation in the Himalayan foreland. *Geol. Soc. Amer. Bull.* 112, 394–412.
- Cerling, T.E., 1992. Use of carbon isotopes in paleosols as an indicator of the P(CO₂) of the paleoatmosphere. *Glob. Biogeochem. Cycles* 6, 307–314.
- Cerling, T.E., Quade, J., 1993. Stable carbon and oxygen isotopes in soil carbonates. In: Swart, P.K., Lohman, K.C., McKenzie, J., Savin, S. (Eds.), *Climate Change in Continental Isotopic Records Monograph 78*. American Geophysical Union, pp. 217–231.
- Cerling, T.E., Quade, J., Wang, Y., Bowman, J.R., 1989. Carbon isotopes in soils and paleosols as ecology and paleoecology indicators. *Nature* 341, 138–139.
- Cerling, T.E., Harris, J.M., MacFadden, B.J., Leakey, M.G., Quade, J., Eisenmann, V., Ehleringer, J.R., 1997. Global vegetation change through the Miocene/Pliocene boundary. *Nature* 389, 153–158.
- Choquette, P., James, N.P., 1990. Limestones – the burial diagenesis environment. In: McIlreath, I.A., Morrow, D.W. (Eds.), *Diagenesis Reprint Series 4*. Geological Association of Canada, Ottawa, pp. 75–112.
- Dansgaard, W., 1964. Stable isotopes in precipitation. *Tellus* 16, 436–468.
- DeCelles, P.G., Gehrels, G.E., Quade, J., Ojha, T.P., Kapp, P.A., Upreti, B.N., 1998. Neogene foreland basin deposits, erosional unroofing, and the kinematic history of the Himalayan fold-thrust belt, western Nepal. *Geol. Soc. Amer. Bull.* 110, 2–21.
- DeCelles, P.G., Robinson, D.M., Quade, J., Ojha, T.P., Garzzone, C.N., Copeland, P., Upreti, B.N., 2001. Stratigraphy, structure, and tectonic evolution of the Himalayan fold-thrust belt in western Nepal. *Tectonics* 20, 487–509.
- DeCelles, P.G., Quade, J., Kapp, P., Fan, M.J., Dettman, D.L., Ding, L., 2007. High and dry in central Tibet during the Late Oligocene. *Earth Planet. Sci. Lett.* 253, 389–401.
- Deutz, P., Montanez, I.P., Monger, H.C., Morrison, J., 2001. Morphology and isotope heterogeneity of Late Quaternary pedogenic carbonates: Implications for paleosol carbonates as paleoenvironmental proxies. *Palaeogeogr. Palaeoclimatol. 166*, 293–317.
- Dewey, J.F., Shackleton, R.M., Chang, C.F., Sun, Y.Y., 1988. The tectonic evolution of the Tibetan plateau. *Philos. Trans. R. Soc. Lond. Ser. A: Math. Phys. Sci.* 327, 379–413.
- Dickson, J.A.D., Coleman, M.L., 1980. Changes in carbon and oxygen isotope composition during limestone diagenesis. *Sedimentology* 27, 107–118.
- Driese, S.G., Mora, C.I., Cotter, E., Foreman, J.L., 1992. Paleopedology and stable isotope chemistry of Late Silurian vertical paleosols, Bloomsburg Formation, Central Pennsylvania. *J. Sediment. Petrol.* 62, 825–841.
- Ekart, D.D., Cerling, T.E., Montanez, I.P., Tabor, N.J., 1999. A 400 million year carbon isotope record of pedogenic carbonate: implications for paleoatmospheric carbon dioxide. *Am. J. Sci.* 299, 805–827.
- Fox, D.L., Koch, P.L., 2004. Carbon and oxygen isotopic variability in Neogene paleosol carbonates: constraints on the evolution of the C-4-grasslands of the Great Plains, USA. *Palaeogeogr. Palaeoclimatol. Palaeoecol.* 207, 305–329.
- Garzzone, C.N., Dettman, D.L., Quade, J., DeCelles, P.G., Butler, R.F., 2000. High times on the Tibetan Plateau: paleoelevation of the Thakkhola graben, Nepal. *Geology* 28, 339–342.
- Garzzone, C.N., Dettman, D.L., Horton, B.K., 2004. Carbonate oxygen isotope paleoaltimetry: evaluating the effect of diagenesis on paleoelevation estimates for the Tibetan plateau. *Palaeogeogr. Palaeoclimatol. Palaeoecol.* 212, 119–140.
- Ghosh, P., Adkins, J., Affek, H., Balta, B., Guo, W.F., Schauble, E.A., Schrag, D., Eller, J.M., 2006. C-13–O-18 bonds in carbonate minerals: a new kind of paleothermometer. *Geochim. Cosmochim. Acta* 70, 1439–1456.
- Guillot, S., Garzanti, E., Baratoux, D., Marquer, D., Maheo, G., de Sigoyer, J., 2003. Reconstructing the total shortening history of the NW Himalaya. *Geochim. Geophys. Geost.* 4.
- He, S., Kapp, P., DeCelles, P.G., Gehrels, G.E., Heizler, M., 2007. Cretaceous–Tertiary geology of the Gangdese Arc in the Linzhou area, southern Tibet. *Tectonophysics* 433, 15–37.

- IAEA, 2005. Isotope Hydrology Database. International Atomic Energy Agency.
- Jacobsen, S.B., Kaufman, A.J., 1999. The Sr, C and O isotopic evolution of Neoproterozoic seawater. *Chem. Geol.* 161, 37–57.
- Kapp, P., DeCelles, P.G., Leier, A.L., Fabijanic, J.M., He, S., Pullen, A., Gehrels, G.E., 2007. The Gangdese retro-arc thrust belt revealed. *GSA Today* 17, 4–9.
- Kaufman, A.J., Knoll, A.H., 1995. Neoproterozoic variations in the C-isotopic composition of seawater – stratigraphic and biogeochemical implications. *Precambrian Res.* 73, 27–49.
- Kim, S.T., O'Neil, J.R., 1997. Equilibrium and nonequilibrium oxygen isotope effects in synthetic carbonates. *Geochim. Cosmochim. Acta* 61, 3461–3475.
- Kingston, J.D., Marino, B.D., Hill, A., 1994. Isotopic evidence for Neogene hominid paleoenvironments in the Kenya Rift Valley. *Science* 264, 955–959.
- Kumar, K., Loyal, R.S., 1987. Eocene ichthyofauna from the Subathu Formation, northwestern Himalaya, India. *J. Palaeontol. Soc. India* 32, 60–84.
- Land, L.S., 1986. Carbonate diagenesis. In: Mumpton, F.A. (Ed.), *Studies in Diagenesis* 1578. U.S. Geological Survey, pp. 129–137.
- Lee, Y., Hisada, K., 1999. Stable isotopic composition of pedogenic carbonates of the Early Cretaceous Shimonoseki Subgroup, western Honshu, Japan. *Palaeogeogr. Palaeoclimatol. Palaeoecol.* 153, 127–138.
- Leeder, M.R., Smith, A.B., Yin, J.X., 1988. Sedimentology, paleoecology and palaeoenvironmental evolution of the 1985 Lhasa to Golmud Geotraverse. *Philos. Trans. R. Soc. Lond. Ser. A: Math. Phys. Sci.* 327, 107–8.
- Leier, A.L., DeCelles, P.G., Kapp, P., Ding, L., 2007a. The Takena formation of the Lhasa terrane, southern Tibet: the record of a Late Cretaceous retroarc foreland basin. *Geol. Soc. Amer. Bull.* 119, 31–48.
- Leier, A.L., Decelles, P.G., Kapp, P., Gehrels, G.E., 2007b. Lower cretaceous strata in the Lhasa Terrane, Tibet, with implications for understanding the early tectonic history of the Tibetan plateau. *J. Sediment. Res.* 77, 809–825.
- Leier, A.L., Kapp, P., Gehrels, G.E., DeCelles, P.G., 2007c. Detrital zircon geochronology of carboniferous–cretaceous strata in the Lhasa terrane, Southern Tibet. *Basin Res.* 19, 361–378.
- Marshall, J.D., 1992. Climatic and oceanographic isotopic signals from the carbonate rock record and their preservation. *Geol. Mag.* 129, 143–160.
- Molnar, P., England, P., Martinod, J., 1993. Mantle dynamics, uplift of the Tibetan Plateau, and the Indian monsoon. *Rev. Geophys.* 31, 357–396.
- Mora, C.I., Driese, S.G., Colarusso, L.A., 1996. Middle to Late Paleozoic atmospheric CO₂ levels from soil carbonate and organic matter. *Science* 271, 1105–1107.
- Morrill, C., Koch, P.L., 2002. Elevation or alteration? Evaluation of isotopic constraints on paleoaltitudes surrounding the Eocene Green River Basin. *Geology* 30, 151–154.
- Najman, Y.M.R., Pringle, M.S., Johnson, M.R.W., Robertson, A.H.F., Wijbrans, J.R., 1997. Laser Ar-40/Ar-39 dating of single detrital muscovite grains from early foreland-basin sedimentary deposits in India: implications for early Himalayan evolution. *Geology* 25, 535–538.
- Ojha, T.P., DeCelles, P.G., Butler, R.F., Quade, J., Magnetic polarity stratigraphy of Neogene Siwalik Group and Dumri Formation, Basin Res. (in review).
- Pagani, M., Zachos, J.C., Freeman, K.H., Tzippe, B., Bohaty, S., 2005. Marked decline in atmospheric carbon dioxide concentrations during the Paleogene. *Science* 309, 600–603.
- Quade, J., Cerling, T.E., 1995. Expansion of C-4 grasses in the Late Miocene of northern Pakistan – evidence from stable isotopes in paleosols. *Palaeogeogr. Palaeoclimatol. Palaeoecol.* 115, 91–116.
- Quade, J., Roe, L.J., 1999. The stable-isotope composition of early ground-water cements from sandstone in paleoecological reconstruction. *J. Sediment. Res.* 69, 667–674.
- Quade, J., Roe, L., DeCelles, P.G., Ojha, T.P., 1997. The late Neogene Sr-87/Sr-86 record of lowland Himalayan rivers. *Science* 276, 1828–1831.
- Quade, J., Garzzone, C., Eiler, J., 2007a. Paleoelevation reconstruction using pedogenic carbonates, Paleoaltimetry: geochemical and thermodynamic approaches. *Rev. Mineral. Geochem.* 66, 53–87.
- Quade, J., Rech, J.A., Latorre, C., Betancourt, J.L., Gleeson, E., Kalin, M.T.K., 2007b. Soils at the hyperarid margin: the isotopic composition of soil carbonate from the Atacama Desert, Northern Chile. *Geochim. Cosmochim. Acta* 71, 3772–3795.
- Romanek, C.S., Grossman, E.L., Morse, J.W., 1992. Carbon isotopic fractionation in synthetic aragonite and calcite – effects of temperature and precipitation rate. *Geochim. Cosmochim. Acta* 56, 419–430.
- Rosales, I., Quesada, S., Robles, S., 2001. Primary and diagenetic isotopic signals in fossils and hemipelagic carbonates: the Lower Jurassic of northern Spain. *Sedimentology* 48, 1149–1169.
- Rowley, D.B., Currie, B.S., 2006. Palaeo-altimetry of the late Eocene to Miocene Lunpola basin, central Tibet. *Nature* 439, 677–681.
- Rush, P.F., Chafetz, H.S., 1990. Fabric-retentive nonluminescent brachiopods as indicators of original delta-C-13 and delta-O-18 composition – a test. *J. Sediment. Petrol.* 60, 968–981.
- Sakai, H., 1983. Geology of the Tansen Group of the Lesser Himalaya in Nepal. *Mem. Fac. Sci. Kyushu Univ.* 25, 27–74.
- Solomon, S.T., Walkden, G.M., 1985. The application of cathodoluminescence to interpreting the diagenesis of an ancient calcrete profile. *Sedimentology* 32, 877–896.
- Tandon, S.K., Andrews, J.E., 2001. Lithofacies associations and stable isotopes of palustrine and calcrete carbonates: examples from an Indian Maastrichtian regolith. *Sedimentology* 48, 339–355.
- Tapponnier, P., Zhiqin, X., Roger, F., Meyer, B., Arnaud, N., Wittlinger, G., Jingsui, Y., 2001. Oblique stepwise rise and growth of the Tibet plateau. *Science* 294, 1671–1677.
- Veizer, J., Ala, D., Azmy, K., Bruckschen, P., Buhl, D., Bruhn, F., Carden, G.A.F., Diener, A., Ebner, S., Godderis, Y., Jasper, T., Korte, C., Pawellek, F., Podlaha, O.G., Strauss, H., 1999. Sr-87/Sr-86, delta C-13 and delta O-18 evolution of Phanerozoic seawater. *Chem. Geol.* 161, 59–88.
- Wenzel, B., 2000. Differential preservation of primary isotopic signatures in silurian brachiopods from northern Europe. *J. Sediment. Res.* 70, 194–209.
- Wright, V.P., Peeters, C., 1989. Origins of some Early Carboniferous calcrete fabrics revealed by cathodoluminescence – implications for interpreting the sites of calcrete formation. *Sedimentary Geology* 65, 345–353.
- Yin, A., Harrison, T.M., 2000. Geologic evolution of the Himalayan–Tibetan orogen. *Ann. Rev. Earth Planet. Sci.* 28, 211–280.
- Yin, J.X., Xu, J.T., Liu, C.J., Li, H., 1988. The Tibetan plateau – regional stratigraphic context and previous work. *Philos. Trans. R. Soc. Lond. Ser. A: Math. Phys. Sci.* 327, 5–8.
- Zachos, J., Pagani, M., Sloan, L., Thomas, E., Billups, K., 2001. Trends, rhythms, and aberrations in global climate 65 Ma to present. *Science* 292, 686–693.